Porous sulfurized poly(acrylonitrile) nanofiber as a long-life and high-capacity cathode for lithium–sulfur batteries

Keyao Wang [b,1], Shunlong Ju [b,1], Qili Gao [b], Guanglin Xia [b], Gaofeng Wang [a], Haixia Yan [a], Linxi Dong [a,*], Zunxian Yang [c,*], Xuebin Yu [b,a,**]

[a] Key Laboratory of RF Circuits and System of Ministry of Education, Electronic and Information College of Hangzhou Dianzi University, Hangzhou 310018, China
[b] Department of Materials Science, Fudan University, Shanghai 200433, China
[c] National & Local United Engineering Laboratory of Flat Panel Display Technology, Fuzhou University, Fuzhou 350002, China

A B S T R A C T

Lithium–sulfur (Li–S) batteries have attracted great interest for next-generation batteries owing to their high capacity density and low cost. However, the drawbacks of the low conductivity of sulfur, serious "shuttle effect" and huge volume expansion during the charging/discharging cycles greatly limit their practical applications. In this work, we report the synthesis of porous sulfurized poly(acrylonitrile) (PAN/S) nanofibers via thermal treatment of PAN/poly(methyl methacrylate) (PMMA) nanofibers with elemental sulfur, resulting in 48 wt% of covalently bound sulfur formed in the composite. The unique porous structure of nanofibers enables enhanced diffusion dynamics of ions and electrons, thus improving the reactivity and conductivity of sulfur. As a consequence, the porous PAN/S cathode delivers a high reversible capacity of 1144 mA h g^{-1} after 100 cycles at a current rate of 0.2 C and a high rate performance with a reversible discharge capacity of 794 mA h g^{-1} at 2 C after 500 cycles.

© 2020 Elsevier B.V. All rights reserved.

1. Introduction

Lithium secondary batteries have been widely used in electric vehicle and grid storage applications [1,2]. However, the existing commercial batteries cannot fully meet the requirements for these fields [3–5]. Developing new electrode materials, especially cathode materials, is the key to getting better battery systems with higher energy density and lower cost [4]. In recent years, Lithium–sulfur (Li–S) batteries, of which the cathode is sulfur, have attracted great attention in both scientific and industrial fields because of their high reversible specific capacity (1672 mA h g^{-1}), nontoxicity, and low cost of sulfur resources [6–9]. However, the development of Li–S batteries is limited due to the low conductivity, serious "shuttle effect" and huge volume expansion of sulfur cathode during charge and discharge cycles [10–13].

Combining sulfur with various carbon-based materials, such as grapheme [14,15], nanostructured carbonaceous materials [16–24] and silicon–carbon materials [18,25], to obtain C/S composites is an effective approach to improve the conductivity of the cathode. However, the volume expansion and shuttle effect can only be alleviated to a certain extent. Besides, C/S composite cathodes are not suitable in carbonate-based electrolytes, which are typically used in commercial Li-ion batteries [6,26–28]. Polysulfides would be consumed by carbonates based solvents, which will result in sulfur inactivity entirely [29–31]. To address this limitation, new approaches must be announced to ensure the sulfur cathode that can charge and discharge with high efficiency in carbonate-based electrolytes [32].

In 2002, Wang et al. firstly reported sulfurized polyacrylonitrile (PAN/S) composites as an appealing cathode material in Li–S batteries [33]. In the PAN/S composite, sulfur is covalently bound to the polymer backbones of PAN via thermal treatment of PAN particles and excess sulfur powder at a temperature above 300 °C [34–37]. During discharge, the solid-solid reaction mechanism suggests that no polysulfide ions are formed [38]. Therefore, the dissolution of reaction intermediates, i.e., shuttle effect, was reported to be completely suppressed in organic carbonate-based electrolytes [39]. By using PAN/S cathode, high sulfur utilization, high Coulombic efficiency and excellent cycling stability can be obtained [35–37,40,41].

* Corresponding authors.
** Corresponding author at: Key Laboratory of RF Circuits and System of Ministry of Education, Electronic and Information College of Hangzhou Dianzi University, Hangzhou 310018, China.
 E-mail addresses: donglinxi@hdu.edu.cn (L. Dong),
yangzunxian@hotmail.com (Z. Yang), yuxuebin@fudan.edu.cn (X. Yu).
[1] These authors contributed equally to this work

However, the insufficient chemical bonding sites leads to the low sulfur content (~40 wt%) of PAN/S composite. Tailored porous structures with optimal porosity and high specific surface area is an ideal option to alleviate this issue. Besides, it can provide directed diffusion pathways for ions, and thus improves the electrical and ionic conductivity of the cathode.

In this work, we developed porous PAN/S nanofibers which were synthesized via electrospinning and subsequent calcination. The PAN/poly(methyl methacrylate) (PMMA) nanofibers that was collected by electrospinning was heated with excess sulfur power to obtain porous PAN/S. The porous morphology of nanofibers increase the reactive site for sulfur, and enlarge the contact area between the electrolyte and the active material. As a result, the PAN/S cathode delivers stable charge/discharge cycling and high rate performance, enabling it an ideal candidate for Li–S batteries.

2. Experimental section

PAN (molecular weight of 150,000) and PMMA (molecular weight of 120,000) ratio was set at 7:1. PAN/PMMA powder (800 mg) was added into 10 ml of N, N-dimethyl formamide (DMF) and then stirred for 24 h to obtain the PAN/PMMA solution. For comparison, 800 mg of PAN powder was added into10 ml of DMF to obtain pure PAN solution.

The PAN/PMMA and pure PAN solutions were absorbed in an injection syringe and subjected to electrospinning. A constant volume flow rate of 0.3 ml h^{-1} was controlled with a syringe-type infusion pump. The distance between the steel needle to the collector was 15 cm. The as-spun nanofibers were then vacuum treated in an oil bath pan at 80 °C for 12 h to ensure that the solvent was fully drained. The as-collected nanofibers were mixed with excess sulfur, and the resulting mixture was heat-treated in a nitrogen atmosphere at a temperature of 300 °C for 4 h at a heating rate of 2 °C min^{-1}. In the heating process, PAN was reacted with sulfur and then dehydrogenated to form PAN/S [42]. Carbon double bonds were sulfurized, while PMMA decomposed to form porous morphology, finally forming porous PAN/S nanofibers [43]. The as-collected nanofibers synthesized using pure PAN solution were also heated using the same parameters, resulting the formation of non-porous PAN/S nanofibers.

The morphology and structure of the porous nanofibers were characterized by X-ray diffraction (XRD), scanning electron microcopy (SEM), transmission electron microscopy (TEM), Raman spectroscopy, X-ray photoelectron spectroscopy (XPS), and nitrogen absorption/desorption isotherms (BET technique). The XRD patterns were recorded in the 2θ range from 10° to 80° at a scan rate of 5 min^{-1}. JEOL 7500FA and JEOL 2011F FE were used to obtain the TEM and SEM images, respectively. Raman spectra, XPS spectra, and BET were obtained using a NEXUS 670 FT-IR Raman spectrometer, Thermo ESCALAB 250XIXPS system, and NOVA 4200e instrument, respectively. The sulfur content in the composite was measured with a Vario Micro Cube Elemental Analyzer.

All cells (2032 coin-type cells) were assembled inside a glovebox filled with high-purity argon with lithium foil as the anode. The as-prepared active materials, Ketjen Black, and carboxymethyl cellulose binder were mixed at a weight ratio of 70:20:10 to obtain the slurry, which was used as coating on the aluminum foil to prepare the cathode. The coated foil was dried at 70 °C in a vacuum for 12 h. Approximately 1 M of lithium hexafluorophosphate(LiPF$_6$) in propylene carbonate (PC):ethylene carbonate (EC):diethyl carbonate (DEC) = 1:4:5 was used as organic carbonate electrolyte. The cells were tested galvanostatically on a LAND-CT2001C test system at a potential interval of 1.0–3.0 V. The specific capacity was calculated on the basis of the sulfur content ratio in the composite nanofibers. Cyclic voltammetric measurements were executed using an electrochemical work station at a scan rate of 0.1 mV s^{-1}.
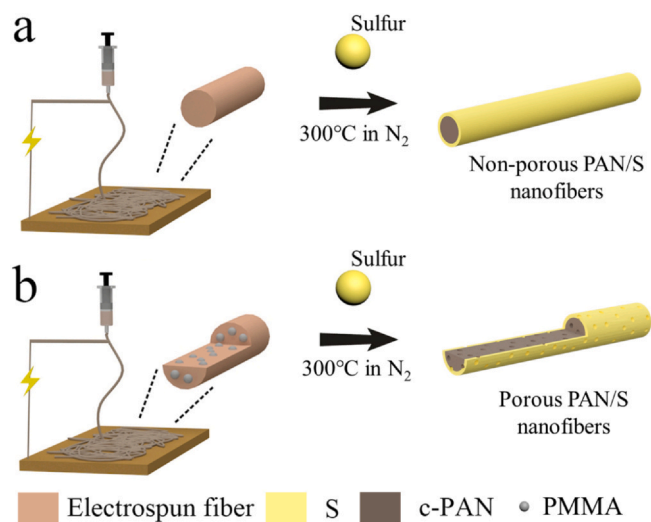
Scheme 1. Schematic illustration of the synthetic process for the (a) non-porous PAN/S nanofibers and (b) porous PAN/S nanofibers.

3. Results and discussion

The synthesis of the PAN/S nanofibers is schematically illustrated in Scheme 1. The ratio of PMMA to PAN in the electrospinning solution was 1:7. The porous PAN/S nanofibers were prepared by electrospinning the PAN/PMMA solution, followed by thermal treatment at 300 °C to allow the reaction of PAN with sulfur and to decompose PMMA to form a porous structure.

The morphological and structural features of porous PAN/S nanofibers were characterized by SEM, TEM, XRD, Raman spectroscopy, XPS, and BET. The SEM image in Fig. 1a reveals that the diameter of the electrospun PAN/PMMA nanofibers ranges from 200 nm to 300 nm. After heat treatment with S powder, the porous PAN/S nanofibers present relatively smooth surface and uniform morphology with some pores both on the surface and in the interior (Fig. 1c and d). The porous structure is formed by thermal elimination of PMMA during heating process [44]. These nanofibers also show a diameter ranging from 200 nm to 300 nm. As compared, the non-porous PAN/S nanofibers synthesized by using pure PAN exhibit smooth surface and uniform morphology without the formation of pores both on the surface and in the interior (Fig. 1b).

The TEM image in Fig. 2a reveals the porosity of the nanofibers. The holes are well dispersed with sizes of approximately 10–20 nm. This structural feature can effectively improve the contact between the cathode and the electrolyte and thus enhance the conductivity of ions and electrons. The corresponding EDX element mapping in Fig. 2b, c, and d shows that both carbon and sulfur elements in the composite are distributed homogeneously.

Fig. 3a shows the XRD patterns of the partially carbonized porous PAN/S nanofibers(c-PAN/S) and PAN without sulfur (c-PAN) and pristine sulfur for comparison. The broad diffraction peak of c-PAN/S at 25° well matches with the peak of c-PAN but not with the peak of pristine sulfur. This finding indicates that PAN and sulfur are successfully mixed in the composite, and sulfur is dispersed in the PAN matrix in an amorphous state [37,45].

Fig. 3b reveals the Raman spectra of porous PAN/S nanofibers. On the basis of previous studies, the peaks at 170 cm^{-1}, 460 cm^{-1} and 920 cm^{-1} are assigned to the C–S, S–S and S–S bonds, respectively, demonstrating the chemical bond of sulfur and PAN [46]. Moreover, the spectrum shows two peaks at 1350 cm^{-1} and 1580 cm^{-1}, which correspond to the D band and G band, respectively. This finding indicates the amorphous structure of the composite [46].
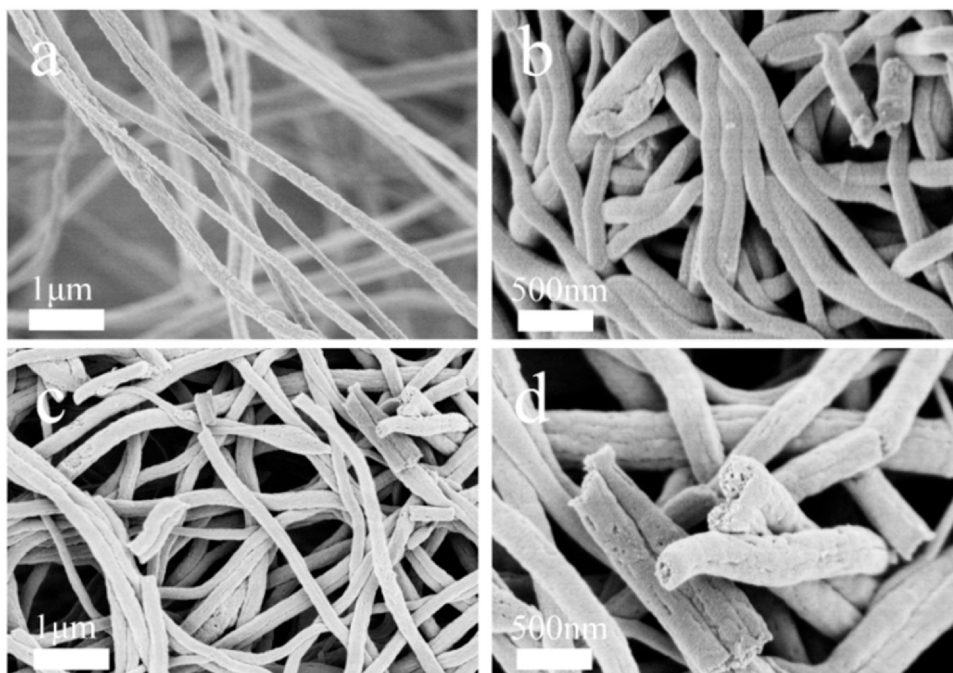
Fig. 1. SEM images of electrospun PAN/PMMA nanofibers(a), non-porous PAN/S nanofibers(b) and porous PAN/S nanofibers(c,d).
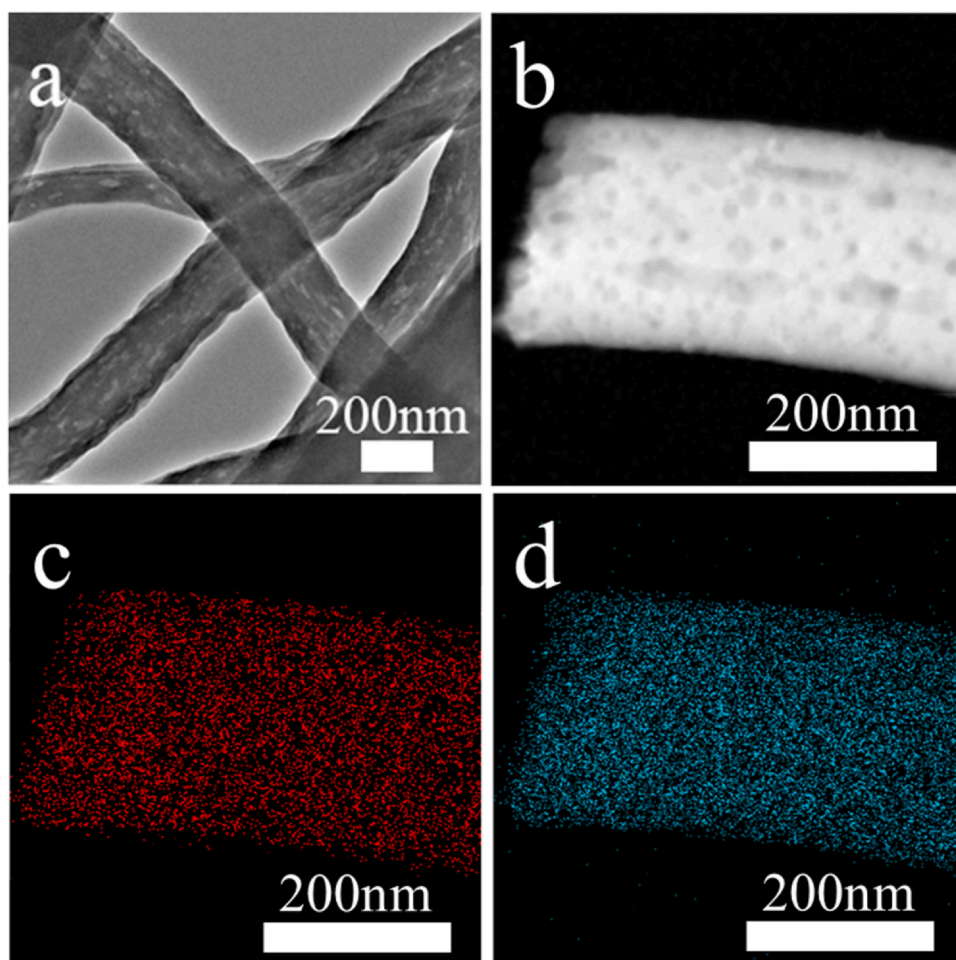

Fig. 2. (a) TEM image of porous PAN/S nanofibers, (b,c,d) EDS mapping of porous PAN/S nanofibers; (c) C element (d) S element.
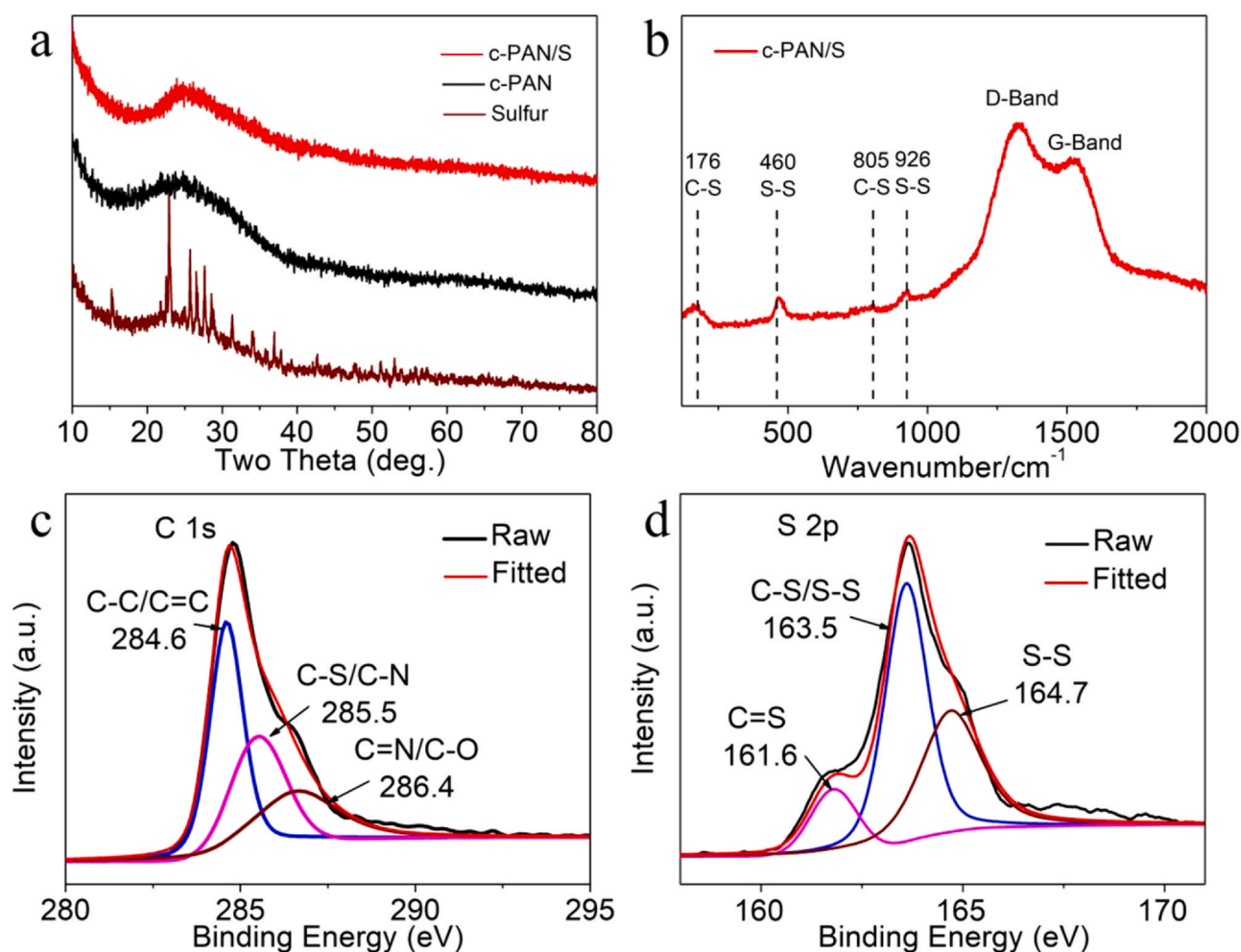
Fig. 3. (a) XRD patterns of porous PAN/S nanofibers (c-PAN/S), (b) Raman spectrum of porous PAN/S nanofibers, (c,d) XPS of C and S element.

The XPS results are shown in Fig. 3c and 3d. In Fig. 3c, the C 1s spectrum can be divided into three sub-peaks. The main peak at 284.6 eV can be attributed to the sp²-hybridized carbon [47]. The peak at 285.5 eV corresponds to the C–S bonds obtained by the reaction of sulfur and PAN during the heating process [47]. The minor peak at 286.4 eV corresponds to the C=N bonds in cycled PAN/S or C–O bonds formed by small range of oxidation reaction during the heating process [48]. It indicates that the sulfur is chemically reacted with PAN framework. The S 2p spectra in Fig. 3d reveals that the main peak can be split into two peaks at 163.5 eV and 164.7 eV, respectively. The peak at 163.5 eV (S 2p$_{3/2}$) can be attributed to the single bonded sulfur species (C–S, S–S), i.e. thioethers, thiols, or di- or polysulfides [49,50]. The peak at 161.6 eV corresponds to sulfur species with a double bond to carbon(C=S), i.e., thioamides, thioketones, or thioureas [51,52]. It demonstrates that the sulfur reacts with PAN framework in different places, which lead to the formation of different kinds of chemical bonds between C and S atoms and the PAN/S composites contained various C, S functional groups [32].

The specific surface areas of non-porous and porous PAN/S nanofibers were measured via N$_2$ adsorption measurements (Fig. S1). It reveals that the porous PAN/S nanofibers exhibit considerably larger surface area than non-porous PAN/S nanofibers (65 m^2 g^{-1} vs. 11 m^2 g^{-1}), indicating that the formation of PMMA-derived porous structure could increase the contact of active material in the cathode and electrolyte.

The electrochemical performance of the porous PAN/S nanofibers as cathodes was evaluated, as shown in Fig. 4. The sulfur contents in the non-porous and porous PAN/S nanofibers are confirmed to be 40% and 48%, respectively. Fig. 4a shows the cyclic voltammograms of the porous PAN/S nanofiber cathode at a scan rate of 0.1 mV s^{-1}. One cathodic peak is observed in the first cycle at 1.3 V. This voltage hysteresis is related to cleavage of S–S bonds adjacent to the carbon ring, which need to input higher energy [39,53]. In the next cycle, the oxidation peak is at 1.7 V and the reduced peak is at 2.3 V. The one pair feature of anodic/cathodic peaks implies the elimination of high-order lithium polysulfides, which probably because active sulfur existed principally as S$_3$ or S$_2$ attached to the adjacent carbon backbone [53,54]. These basic electrochemical characteristics are similar to the results observed from the reported PAN/S composite [53–55].

Fig. 4b displays the galvanostatic charge–discharge curves in the 1st, 2nd, 3rd, and 100th cycles for the porous PAN/S nanofibers. The curves of the nanofiber cathode show a one-stage potential profile with a long plateau at a potential of 1.7 V at the first discharge with a discharge capacity of 1692 mA h g^{-1}. The plateau shift to 1.9 V after the second cycle with discharge capacities of 1403 mA h g^{-1}, 1385 mA h g^{-1}, and 1144 mA h g^{-1} for the 2nd, 3rd, and 100th cycle, respectively. As for charge process, the cathode show a higher single-charge plateau at a potential over 2.3 V, giving charge capacities of 1421 mA h g^{-1}, 1387 mA h g^{-1}, 1372 mA h g^{-1} and 1144 mA h g^{-1} in the 1st, 2nd, 3rd, and 100th cycle, respectively, indicating the high reversible capacity of the porous PAN/S nanofiber cathode.

Fig. 4c shows the discharge cycling performance and coulombic efficiency of the porous PAN/S nanofiber cathode under a current
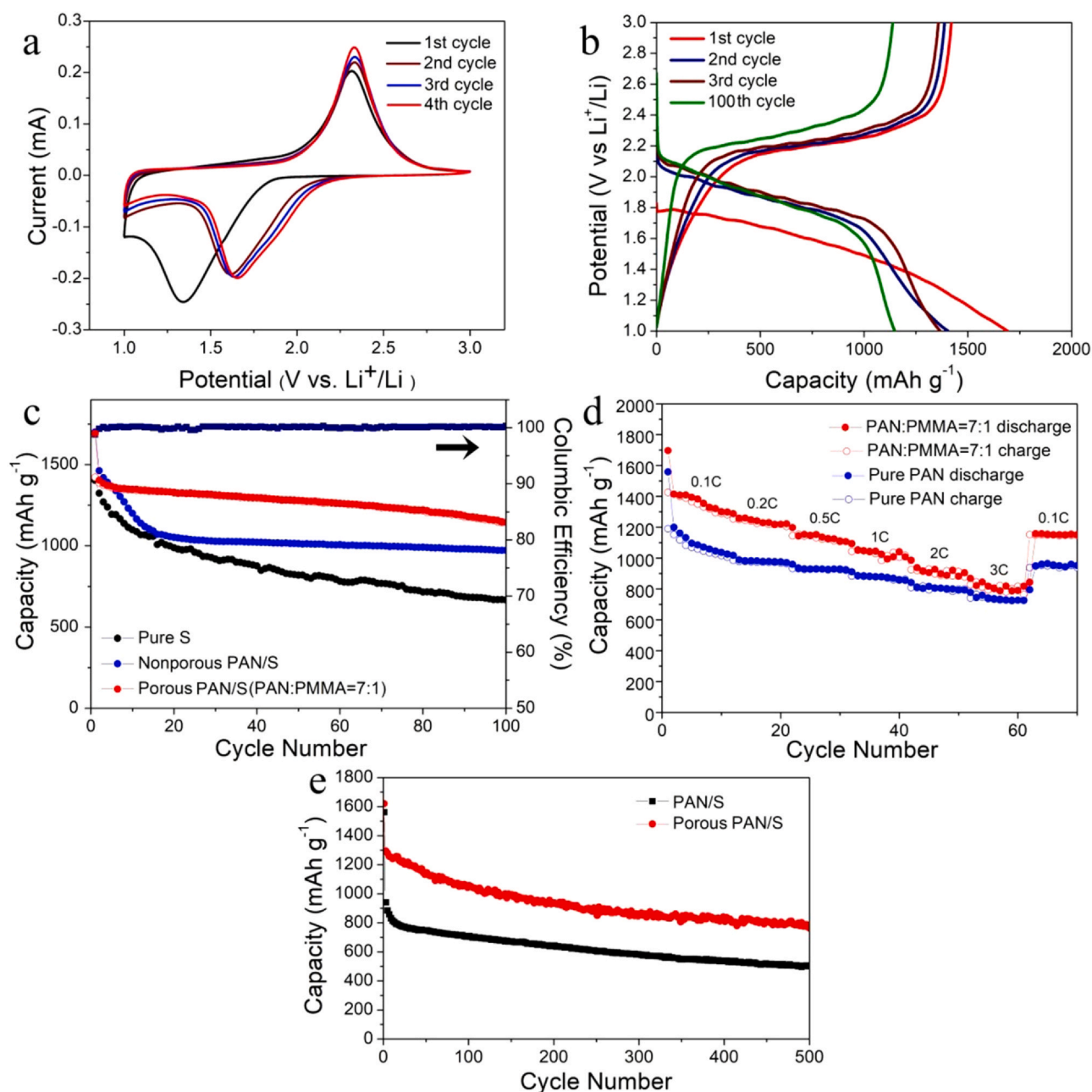
Fig. 4. (a) Cyclic voltammograms curves for the porous PAN/S nanofiber cathode at a scan rate of 0.1 mV s^{-1}; (b) Galvanostatic discharge/charge voltage profiles for the porous PAN/S nanofiber cathode with selected cycles at 0.2 C; (c) Cycling performance of the porous PAN/S nanofiber cathode at 0.2 C as compared with the pure S and non-porous PAN/S cathode; (d) Rate performance for the porous PAN/S nanofiber cathode at current densities from 0.1 C to 3 C; (e) Cycling performance of the porous PAN/S nanofiber cathode at 2 C as compared with the non-porous PAN/S cathode.

density of 0.2 C. Clear capacity decay is only observed after the first cycle, followed by a relatively stable discharge capacity. The main reason for the capacity loss after the first cycle could be attributed to the formation of the SEI film [56,57]. The discharge capacity at the 100th cycle is high to 1144 mA h g$_{sulfur}^{-1}$, and the Columbic efficiency reaches to ~100%. This finding confirms the effectiveness of the porous PAN/S nanofiber architecture in improving sulfur reactivity. For the non-porous PAN/S nanofibers, although the initial capacity is 1700 mA h g$_{sulfur}^{-1}$, it decreases sharply to 1052 mA h g$_{sulfur}^{-1}$ after 20 cycles and further decreases to 972.5 mA h g$_{sulfur}^{-1}$ after 100 cycles. The pure sulfur cathode, in which the ether electrolytes are used, demonstrated even worse capacity retention ability.

The rate capacities of porous PAN/S nanofibers are shown in Fig. 4d. The results display that the discharge capacity decreases

gradually during the initial few cycles at 0.1 C, and then became stable in further cycles. At higher C-rate, the capacity decreases regularly. When the C-rate is switched back from 3 C to 0.2 C, the discharge capacity increased up to 1158 mA h g$_{sulfur}^{-1}$, indicating the excellent recovery of discharge capacity. These results confirm that the porous PAN/S nanofibers have good electrochemical cycle stability and structure stability even under large current density. In addition, the sample with a ratio of PAN:PMMA = 7:1 showed better performance than that without the addition of PMMA, indicating the importance of PMMA on improving the properties of the composite. The effect of various ratios of PAN/PMMA on the electrochemical properties of PAN/S nanofiber was investigated, and the results are shown in Figs. S2 and S3. The best ratio of PAN/PMMA that can effectively balance the advantages and drawbacks of PMMA for the
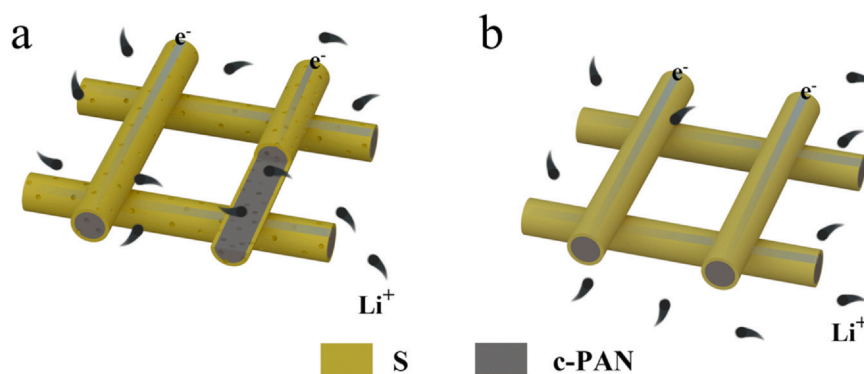
Fig. 5. Schematic illustration of the structural advantage of (a) porous PAN/S nanofibers compared to (b) non-porous PAN/S nanofibers as cathode materials.

production of porous structure is found to be 7:1. When a small amount of PMMA is added, the porous structure formed is not enough to enhance the electrochemical performance. However, after adding excessive amount of PMMA, the carbon matrix is destroyed during the synthesis.

The cycling performance of the porous PAN/S nanofibers are further investigated as shown in Fig. 4e. At a high current rate of 2 C, the initial discharge capacity of porous PAN/S nanofibers is determined to be approximately 1620 mA h g_{sulfur}^{-1}, and after 500 cycles, it could still be maintained at 794 mA h g_{sulfur}^{-1}. However, the capacity of non-porous PAN/S nanofibers could only maintain at 522 mA h g_{sulfur}^{-1}. On the basis of the above results, it can be clearly concluded that the porous PAN/S nanofiber cathode possesses significantly improved capacity and cycling performance. This excellent performance is attributed to the porous nanofiber structure, which plays an important role in enhancing the directed diffusion pathways for ions and electrons [32]. Moreover, to demonstrate the structural integrity of porous PAN/S nanofibers, the morphology of the cathode after cycling is studied. As shown in Fig. S5, the well preserved porous structure after long-term cycling demonstrates the outstanding structural integrity, which contributes to the improved cycling stability.

Fig. S4 shows the comparison of EIS between porous and non-porous PAN/S nanofibers after a few cycles using 2 electrode system. The Nyquist plot is composed of the bulk resistance of the electrolyte at high frequency, charge transfer resistance at middle frequency and Warburg impedance at low frequency. The corresponding calculated impendence values are given in Table S1. In the middle frequency region, the charge transfer resistances of porous PAN/S is 17.6 Ω, while the charge transfer resistances of non-porous PAN/S is 87.82 Ω. A much smaller value of porous PAN/S indicates that the porous structure of the composite could reduce the charge transfer resistance. Such results further confirm that the porous structure improves the ion and electron conductivity and enables better performance in capacity and cycle stability.

Compared with the previously reported performance for the PAN/S fiber materials (Table S2), the porous PAN/S nanofibers attain outstanding electrochemical performance because of their unique structural morphology. The schematic illustration for the improvement is shown in Fig. 5. The porous PAN/S nanofibers create a nanoscaled crack-free cathode coating, which result in a relatively large specific surface area and effective conduction networks for the diffusion of electrons and lithium ions. Moreover, compared with the non-porous PAN/S nanofibers, the porous morphology is able to provide more sufficient contact with the electrolyte and further create a convenient passage way for Li$^+$ and electron to react with active materials more sufficiently, resulting in the enhancement of ion and electron conductivity and reactivity of sulfur. Such morphology effectively improves the charge/discharge capacities especially at high current. In addition, the bonds between carbon and sulfur in the PAN/S composites indicate that polysulfides only emerge in a short-chain form and have low solubility in the organic carbonate-based electrolytes, thereby preventing the "shuttle effect" of polysulfides and improving cycle ability. All these features guarantee the porous PAN/S nanofibers an excellent electrochemical performance.

4. Conclusions

Porous PAN/S nanofibers were prepared via electrospinning method combined with heat treatment process. The PMMA acts as a pore-forming agent to produce porous morphology, which is beneficial for the diffusion of ions and electrons, thus improving the capacity and cycling performance. The porous PAN/S nanofiber cathode in the carbonate-based electrolyte exhibit high cycle stability (1144 mA h g^{-1} at 0.2 C after 100 cycles, 794 mA h g^{-1} at 2 C after 500 cycles) and Coulombic efficiency (~100%). The creative structure of PAN/S composite combined with the unique working mechanism of PAN/S in carbonate-based electrolyte provide new insights for manufacturing long-life and high-capacity Li–S batteries.

CRediT authorship contribution statement

Keyao Wang: Writing - original draft, Formal analysis, Investigation. **Shunlong Ju**: Writing - review & editing, Validation, Investigation, Formal analysis. **Qili Gao**: Formal analysis, Investigation. **Guanglin Xia**: Formal analysis, Methodology. **Gaofeng Wang**: Formal analysis. **Haixia Yan**: Visualization. **Linxi Dong**: Formal analysis, Validation, Resources. **Zunxian Yang**: Formal analysis, Methodology, Resources. **Xuebin Yu**: Supervision, Writing - review & editing, Resources, Funding acquisition, Project administration.

Declaration of Competing Interest

The authors declare that they have no known competing financial interests or personal relationships that could have appeared to influence the work reported in this paper.

Acknowledgements

Appendix A. Supporting information

Supplementary data associated with this article can be found in the online version at doi:10.1016/j.jallcom.2020.158445.

References

[1] M. Armand, J.M. Tarascon, Building better batteries, Nature 451 (2008) 652–657.

[2] Y. Liu, H. Pan, M. Gao, Q. Wang, Advanced hydrogen storage alloys for Ni/MH rechargeable batteries, J. Mater. Chem. 21 (2011) 4743–4755.

[3] P. Wang, M. Gao, H. Pan, J. Zhang, C. Liang, J. Wang, P. Zhou, Y. Liu, A facile synthesis of Fe3O4/C composite with high cycle stability as anode material for lithium-ion batteries, J. Power Sources 239 (2013) 466–474.

[4] S.M. Zhang, H.T. Gu, H.G. Pan, S.H. Yang, W.B. Du, A novel strategy to suppress capacity and voltage fading of Li- and Mn-rich layered oxide cathode material for lithium-ion batteries, Adv. Energy Mater. 1 (2016) 1601066–1601077.

[5] Y.F. Liu, H.G. Pan, M.X. Gao, R. Li, Y.Q. Lei, Effect of Co content on the structural and electrochemical properties of the La0.7Mg0.3Ni3.4−xMn0.1Cox hydride alloys: II. Electrochemical properties, J. Alloy. Compd. 376 (2004) 304–313.

[6] J. Ye, F. He, J. Nie, Y. Cao, H. Yang, X. Ai, Sulfur/carbon nanocomposite-filled polyacrylonitrile nanofibers as a long life and high capacity cathode for lithium–sulfur batteries, J. Mater. Chem. A 3 (2015) 7406–7412.

[7] A. Manthiram, Y. Fu, Y.S. Su, Challenges and prospects of lithium–sulfur batteries, Acc. Chem. Res. 46 (2012) 1125–1134.

[8] Y. Yang, G. Zheng, Y. Cui, Nanostructured sulfur cathodes, Chem. Soc. Rev. 42 (2013) 3018–3032.

[9] C. Lin, L.L. Shaw, Recent advances in lithium–sulfur batteries, J. Power Sources 267 (2014) 770–783.

[10] C. Huang, J. Xiao, Y. Shao, J. Zheng, W.D. Bennett, D. Lu, L.V. Saraf, M. Engelhard, L. Ji, J. Zhang, Manipulating surface reactions in lithium-sulphur batteries using hybrid anode structures, Nat. Commun. 5 (2014) 3015.

[11] S. Xin, L. Gu, N.H. Zhao, Y.X. Yin, L.J. Zhou, Y.G. Guo, L.J. Wan, Smaller sulfur molecules promise better lithium-sulfur batteries, J. Am. Chem. Soc. 134 (2012) 18510–18513.

[12] J. Guo, Y.H. Xu, C. Wang, Sulfur-impregnated disordered carbon nanotubes cathode for lithium–sulfur batteries, Nano Lett. 11 (2011) 4288–4294.

[13] Y. Yan, Y.X. Yin, S. Xin, Y.G. Guo, L.J. Wan, Ionothermal synthesis of sulfur–doped porous carbons hybridized with graphene as superior anode materials for lithium-ion batteries, Chem. Commun. 48 (2012) 10663–10665.

[14] H. Wang, Y. Yang, Y. Liang, J.T. Robinson, Y. Li, A. Jackson, Y. Cui, H. Dai, Graphene-wrapped sulfur particles as a rechargeable lithium–sulfur battery cathode material with high capacity and cycling stability, Nano Lett. 11 (2011) 2644–2647.

[15] J.S. Yeon, S. Yun, J.M. Park, H.S. Park, Surface-modified sulfur nanorods immobilized on radially assembled open-porous graphene microspheres for lithium–sulfur batteries, ACS Nano 13 (2019) 5163–5171.

[16] S. Yun, S.M. Bak, S. Kim, J.S. Yeon, M.G. Kim, X.Q. Yang, P.V. Braun, H.S. Park, Rational design of hierarchically open-porous spherical hybrid architectures for lithium-ion batteries, Adv. Energy Mater. 9 (2019) 1802816.

[17] M. Oschatz, S. Thieme, L. Borchardt, M.R. Lohe, T. Biemelt, J. Brückner, H. Althues, S. Kaskel, A new route for the preparation of mesoporous carbon materials with high performance in lithium–sulphur battery cathodes, Chem. Commun. 49 (2013) 5832–5834.

[18] N. Jayaprakash, J. Shen, S.S. Moganty, A. Corona, L.A. Archer, Porous hollow carbon@sulfur composites for high-power lithium–sulfur batteries, Angew. Chem. Int. Ed. 50 (2011) 5904–5908.

[19] M. Jana, R. Xu, X.B. Cheng, J.S. Yeon, J.M. Park, J.Q. Huang, Q. Zhang, H.S. Park, Rational design of two-dimensional nanomaterials for lithium–sulfur batteries, Energy Environ. Sci. 13 (2020) 1049–1075.

[20] Y.L. Ding, P. Kopold, K. Hahn, P.A. van Aken, J. Maier, Y. Yu, Lithium-sulfur batteries: facile solid–state growth of 3D well-interconnected nitrogen–rich carbon nanotube–graphene hybrid architectures for lithium–sulfur batteries, Adv. Funct. Mater. 26 (2016) 1112–1119.

[21] C. Tang, Q. Zhang, M.Q. Zhao, J.Q. Huang, X.B. Cheng, G.L. Tian, H.J. Peng, F. Wei, Nitrogen-doped aligned carbon nanotube/graphene sandwiches: facile catalytic growth on bifunctional natural catalysts and their applications as scaffolds for high-rate lithium–sulfur batteries, Adv. Mater. 26 (2015) 6100–6105.

[22] X. Ji, K.T. Lee, L.F. Nazar, A highly ordered nanostructured carbon–sulphur cathode for lithium–sulphur batteries, Nat. Mater. 8 (2009) 500–506.

[23] Y. Qu, Z. Zhang, X. Zhang, G. Ren, Y. Lai, Y. Liu, L. Jie, Highly ordered nitrogen–rich mesoporous carbon derived from biomass waste for high-performance lithium–sulfur batteries, Carbon 84 (2015) 399–408.

[24] X. Ji, S. Evers, R. Black, L.F. Nazar, Stabilizing lithium–sulphur cathodes using polysulphide reservoirs, Nat. Commun. 2 (2011) 325.

[25] J. Schuster, G. He, B. Mandlmeier, T. Yim, K.T. Lee, T. Bein, L.F. Nazar, Spherical ordered mesoporous carbon nanoparticles with high porosity for lithium–sulfur batteries, Angew. Chem. Int. Ed. 51 (2012) 3591–3595.

[26] B. Zhang, X. Qin, G.R. Li, X.P. Gao, Enhancement of long stability of sulfur cathode by encapsulating sulfur into micropores of carbon spheres, Energy Environ. Sci. 3 (2010) 1531–1537.

[27] J. Gao, M.A. Lowe, Y. Kiya, H.D. Abruna, Effects of liquid electrolytes on the charge–discharge performance of rechargeable lithium/sulfur batteries: electrochemical and in-situ x-ray absorption spectroscopic studies, J. Phys. Chem. C 115 (2011) 25132–25137.

[28] L. Wang, X.M. He, J.J. Li, M. Chen, J. Gao, C.Y. Jiang, Charge/discharge characteristics of sulfurized polyacrylonitrile composite with different sulfur content in carbonate based electrolyte for lithium batteries, Electrochim. Acta 72 (2012) 114–119.

[29] C. Zhao, L. Liu, H. Zhao, A. Krall, Z. Wen, J. Chen, P. Hurley, J. Jiang, Y. Li, Sulfur–infiltrated porous carbon microspheres with controllable multi-modal pore size distribution for high energy lithium–sulfur batteries, Nanoscale 6 (2013) 882–888.

[30] W. Zhang, D. Qiao, J. Pan, Y. Cao, H. Yang, A.I. Xinping, A Li+-conductive microporous carbon–sulfur composite for Li–S batteries, Electrochim. Acta 87 (2013) 497–502.

[31] J. Song, T. Xu, M.L. Gordin, P. Zhu, D. Lv, Y.B. Jiang, Y. Chen, Y. Duan, D. Wang, Nitrogen-doped mesoporous carbon promoted chemical adsorption of sulfur and fabrication of high-areal-capacity sulfur cathode with exceptional cycling stability for lithium-sulfur batteries, Adv. Funct. Mater. 24 (2014) 1243–1250.

[32] M. Frey, R.K. Zenn, S. Warneke, K. Müller, A. Hintennach, R.E. Dinnebier, M.R. Buchmeiser, Easily accessible, textile fiber-based sulfurized poly(acrylonitrile) as Li/S cathode material: correlating electrochemical performance with morphology and structure, ACS Energy Lett. 2 (2017) 595–604.

[33] J.L. Wang, J. Yang, J.Y. Xie, N.X. Xu, A. Novel, Conductive polymer-sulfur composite cathode material for rechargeable lithium batteries, Adv. Mater. 14 (2002) 13–14.

[34] J.L. Wang, J. Yang, C.R. Wan, K. Du, J.Y. Xie, N.X. Xu, Sulfur composite cathode materials for rechargeable lithium batteries, Adv. Funct. Mater. 13 (2010) 487–492.

[35] J. Fanous, M. Wegner, J. Grimminger, Ä. Andresen, M.R. Buchmeiser, Structure-related electrochemistry of sulfur-poly(acrylonitrile) composite cathode materials for rechargeable lithium batteries, Chem. Mater. 23 (2012) 5024–5028.

[36] A. Konarov, D. Gosselink, T.N.L. Doan, Y. Zhang, Z. Yan, P. Chen, Simple, scalable, and economical preparation of sulfur–PAN composite cathodes for Li/S batteries, J. Power Sources 259 (2014) 183–187.

[37] X.G. Yu, J.Y. Xie, J. Yang, H.J. Huang, K. Wang, Z.S. Wen, Lithium storage in conductive sulfur-containing polymers, J. Electroanal. Chem. 573 (2004) 121–128.

[38] X.F. Wang, Y.M. Qian, L.N. Wang, H. Yang, H.L. Li, Y. Zhao, T.X. Liu, Sulfurized polyacrylonitrile cathodes with high compatibility in both ether and carbonate electrolytes for ultrastable lithium–sulfur batteries, Adv. Funct. Mater. 29 (2019) 1902929.

[39] S.S. Zhang, Understanding of sulfurized polyacrylonitrile for superior performance lithium/sulfur battery, Energies 7 (2014) 4588–4600.

[40] L.C. Yin, J.L. Wang, F.J. Lin, J. Yang, Y. Nuli, Polyacrylonitrile/graphene composite as a precursor to a sulfur-based cathode material for high-rate rechargeable Li-S batteries, Energy Environ. Sci. 5 (2012) 6966–6972.

[41] J.Y. Lei, J.H. Chen, H.M. Zhang, A. Naveed, J. Yang, Y. Nuli, J.L. Wang, High molecular weight polyacrylonitrile precursor for S@pPAN composite cathode materials with high specific capacity for rechargeable lithium batteries, ACS Appl. Mater. Interfaces 12 (2020) 33702–33709.

[42] Z. Wang, Y. Dong, H. Li, Z. Zhao, H.B. Wu, C. Hao, S. Liu, J. Qiu, X.W. Lou, Enhancing lithium-sulphur battery performance by strongly binding the discharge products on amino-functionalized reduced graphene oxide, Nat. Commun. 5 (2014) 5002.

[43] Y. Wu, M. Gao, L. Xiang, Y. Liu, H. Pan, Preparation of mesohollow and microporous carbon nanofiber and its application in cathode material for lithium–sulfur batteries, J. Alloy. Compd. 608 (2014) 220–228.

[44] J.S. Lee, J. Kim, W. Jang, A. Manthiram, Sulfur-embedded activated multichannel carbon nanofiber composites for long-life, high-rate lithium-sulfur batteries, Adv. Energy Mater. 7 (2017) 1601943.

[45] H. Peng, X. Wang, Z. Yan, T. Tan, A. Mentbayeva, Z. Bakenov, Y. Zhang, Enhanced electrochemical performance of sulfur/polyacrylonitrile composite by carbon coating for lithium/sulfur batteries, J. Nanopart. Res. 19 (2017) 348.

[46] X.M. He, L. Wang, W.H. Pu, J.G. Ren, W. Wu, C.Y. Jiang, C.R. Wan, Thermal analysis of sulfurization of polyacrylonitrile with elemental sulfur, J. Therm. Anal. Calorim. 94 (2008) 151–155.

[47] Y.Z. Zhang, S. Liu, G.C. Li, G.R. Li, X.P. Gao, Sulfur/polyacrylonitrile/carbon multi-composites as cathode materials for lithium/sulfur battery in the concentrated electrolyte, J. Mater. Chem. A 2 (2014) 4652–4659.

[48] S. Wei, L. Ma, K.E. Hendrickson, Z. Tu, L.A. Archer, Metal–sulfur battery cathodes based on PAN–SUlfur Composites, J. Am. Chem. Soc. 137 (2015) 12143–12152.

[49] J. Riga, J.J. Verbist, ChemInform Abstract: the Disulfide Group in Organic Compounds: Conformational Dependence of Core and Valence Sulfur Electronic Levels by X-ray Photoelectron Spectroscopy, Chemischer Informationsdienst, 15 Wiley-VCH, 1984.

[50] B.J. Lindberg, K. Hamrin, G. Johansson, U. Gelius, A. Fahlman, C. Nordling, K. Siegbahn, Molecular spectroscopy by means of ESCA II. Sulfur compounds. Correlation of electron binding energy with structure, Phys. Scr. 1 (1970) 286–298.

[51] K.W. Jeon, D.K. Seo, Concomitant thionation and reduction of graphene oxide through solid/gas metathetical sulfidation reactions at high temperatures, Phosphorus Sulfur Silicon Relat. Elem. 189 (2014) 721–737.

[52] J. Peeling, F.E. Hruska, D.M. Mckinnon, M.S. Chauhan, N.S. Mcintyre, ESCA studies of the uracil base. The effect of methylation, thionation, and ionization on charge distribution, Can. J. Chem. 56 (1978) 2405–2411.

[53] Y. Liu, A.K. Haridas, K.K. Cho, Y. Lee, J.H. Ahn, Highly ordered mesoporous sulfurized polyacrylonitrile cathode material for high-rate lithium sulfur batteries, J. Phys. Chem. C 121 (2017) 26172–26179.

[54] S. Wei, L. Ma, K.E. Hendrickson, Z.Y. Tu, L.A. Archer, Metal−sulfur battery cathodes based on PAN−sulfur composites, J. Am. Chem. Soc. 137 (2015) 12143–12152.

[55] T.N.L. Doan, M. Ghaznavi, A. Konarov, Y. Zhang, P. Chen, Cyclability of sulfur/ dehydrogenated polyacrylonitrile composite cathode in lithium–sulfur batteries, J. Solid State Electrochem. 18 (2014) 69–76.

[56] S.S. Zhang, Understanding of sulfurized polyacrylonitrile for superior perfor-mance lithium/sulfur battery, Energies 7 (2014) 4588–4600.

[57] W. Li, X. He, J. Li, G. Jian, J. Guo, C. Jiang, C. Wan, Analysis of the synthesis process of sulphur–poly(acrylonitrile)-based cathode materials for lithium batteries, J. Mater. Chem. 22 (2012) 22077–22081.